Polymer Testing 122 (2023) 108014

Contents lists available at ScienceDirect

Polymer Testing

journal homepage: www.elsevier.com/locate/polytest

Deformation analysis in impact testing of functionally graded foams by the image processing of high-speed camera recordings

Márton Tomin [a], Dániel Török [a], Tamás Pászthy [b], Ákos Kmetty [a,c,*]

[a] Department of Polymer Engineering, Faculty of Mechanical Engineering, Budapest University of Technology and Economics, Műegyetem rkp. 3, H-1111, Budapest, Hungary
[b] Department of Information Technology, University of Miskolc, Egyetem út 17, H-3515, Miskolc - Egyetemváros, Hungary
[c] ELKH–BME Research Group for Composite Science and Technology, Műegyetem rkp. 3, H-1111, Budapest, Hungary

ARTICLE INFO

Keywords:
Impact test
High-speed camera
Image processing
Density gradient
Polymer foam

ABSTRACT

We developed an image processing algorithm and applied it on high-speed camera recordings to characterize the deformation response of three-layered density-graded foam structures subjected to drop weight testing. Different densities (30, 40, 50 and 70 kg/m^3) of weakly cross-linked polyethylene foam sheets were laminated together to achieve varying density distributions along the thickness, and the effect of layer order on the shock absorption capability was evaluated. Foam structures with a higher density top layer and a negative density gradient showed enhanced energy absorption in the initial stage of deformation, which resulted in lower maximum reaction forces. The positive effect of layer order modification was more dominant at higher impact energies. We provided a detailed explanation of the tendencies by investigating the differences in deformation propagation and the changes in the diameter of the deformation zone. The presented method can be utilized to design sports and packaging foam products.

1. Introduction

Weight reduction to decrease material costs and the environmental footprint of transportation is becoming an increasingly important goal for engineers. Therefore, polymeric foams are of paramount importance, as they contribute to weight reduction and have excellent thermal and mechanical properties at the same time [1]. Foams are important not only in the packaging industry [2] but in several other applications as well. They are used in the construction industry for the thermal insulation of buildings [3] and as soundproofing walls for noise reduction [4]. Moreover, their advanced energy-absorbing capacity is also exploited in automotive [5,6] and sports applications [7,8], where they can protect the passengers/athletes from injuries by reducing the shocks during collisions/impacts. Due to their cellular structure, polymer foams show a special material response to loads, especially under compression (see Fig. 1.), when they can absorb a huge amount of energy in the so-called plateau region through cell wall bending and buckling [9,10].

However, in some cases, a homogenous density foam structure is not resistant enough to absorb the energy of the impact, and the resulting excessive cell compaction leads to undesirable material response with high reaction forces (densification zone) [13]. As a result, focus has shifted to developing functionally graded foams that have varying density distribution along the thickness [14]. With the use of a non-uniform cell structure, the stress level of the plateau zone can be increased, and the start of the densification zone can be shifted to higher strain levels, allowing more energy to be absorbed with lower reaction forces.

Several studies in recent years aimed to produce foams with non-uniform density distribution. The approaches presented so far include syntactic foaming [15–17], batch foaming [18,19], compression molding [20], and injection molding of structural foams [21,22], which all result in a continuously varying density.

In the case of syntactic foaming, researchers use micro-balloons distributed in a polymer matrix [15], which mostly results in precisely controlled particle distribution, thus a quasi-homogenous cell structure. However, the achievable mass reduction is relatively low. Gupta [16] used glass micro-balloons and epoxy resin to produce 500–700 kg/m^3 density foams while using the same processing technology, Higuchi et al. [17] achieved 720 and 930 kg/m^3 densities. Both studies came to the conclusion that by changing the density distribution along the thickness, the energy absorption capacity of foams measured in compression tests

* Corresponding author. Department of Polymer Engineering, Faculty of Mechanical Engineering, Budapest University of Technology and Economics, Műegyetem rkp. 3, H-1111, Budapest, Hungary.
E-mail address: kmetty@pt.bme.hu (Á. Kmetty).

https://doi.org/10.1016/j.polymertesting.2023.108014
Received 9 December 2022; Received in revised form 14 March 2023; Accepted 1 April 2023
Available online 3 April 2023

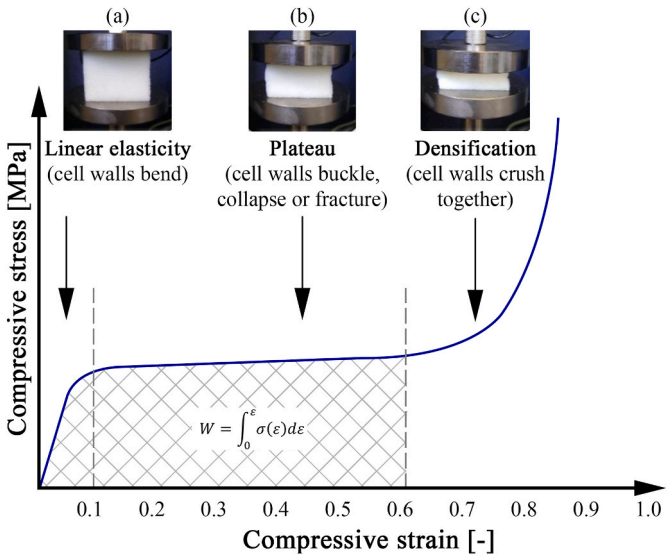

Fig. 1. Typical stress–strain response of a polymer foam to compressive load with the three well-distinguished regions: (a) linear elasticity, (b) plateau, (c) densification (reproduced with general permission of SciELO [11] and permission of Elsevier [12]).

can be increased [16,17].

Similar density reduction was achieved by Cusson et al. [20], who applied different temperatures on both sides of a compression molding system to produce linear low-density polyethylene foams using azodicarbonamide as a chemical blowing agent.

Much higher porosity can be obtained with supercritical gas as a physical blowing agent [18,19]. Mohyeddin and Fereidoon [18] implemented a solid-state batch process, which resulted in foams with a graded porosity foam core and an integral solid skin layer. Another innovative solution was proposed by Yu et al. [19], who batch foamed polymers on a substrate of anodized aluminum oxide film modified with fluorinated silane. First, polymer particles were compressed on the film in a hydraulic press to produce ~1 mm thick plates, and then they were batch foamed in a high-pressure vessel with a $scCO_2$ blowing agent. The cell size of the graded foam near the substrate decreased to a minimum of 2 μm, gradually increasing in an upward direction.

Compared to structural foams with uniform cells, we can also produce products with far higher strength by injection molding structural foams, which have a sandwich structure. Both the foam core and rigid shell layer of these structures are formed during the manufacturing process. Since the wall of the mold is cold, the polymer melt, which gets into contact with the mold surface, solidifies quickly, so the gas cannot expand the polymer there. Most studies using this approach set different temperatures on the two cavity surfaces and investigate the effect of this temperature difference on the thickness ratio of the skin and core layers. Although the transition between the morphology of the shell and core layers is sharp, the achievable density reduction is generally small (~30%) [1,21–23].

The presented articles are limited mainly to the investigation of the morphology with the aim of assessing the applicability and reproducibility of the production method. The limited number of experimental data on the mechanical testing of functionally graded foams and the lack of analysis on their deformation mechanism means that we can mostly conclude the material response from theoretical analysis. Uddin et al. [24] investigated virtual three-layered polyurea foam laminates subjected to quasi-static uniaxial compression and showed that graded laminates could outperform single-density foams in terms of strength and energy absorption. Similar conclusions were found by Koohbor and Kidane [14] from the constitutive modeling of compression testing 4-layer graded polyurethane foam structures. As the numerical simulation of foam behavior at high strain rates requires high computational capacity and complicated parameter fitting [25], only one study is available that investigated in detail the effect of the density gradient on the shock-absorbing capacity at different impact energies. Cui et al. [26] performed finite element simulations for the drop weight tests of functionally graded closed-cell foams. In the impact energy range of 15–30 J, structures with decreasing density from top to bottom showed better shock absorption capacity compared to uniform density foam models. This difference disappeared at higher impact energies as the foam models were completely compressed. Their conclusion assumed that the foam should absorb all the impact energy in the plateau range before densification starts. If this region is reached, the foam will transmit the majority of the energy as a propagating stress wave to the user/product, which should be protected. However, it is important to note that the simulation results were not validated by tests, and the exact deformation response of a varying-density foam structure to impact loads was not studied.

In addition to the production of continuously graded structures in one step during foaming, the generation of discretely graded structures is also a possibility in a two-step manufacturing process. In the case of packaging and sports, sheet extrusion [27] is the most widespread industrial technology to produce normal foam sheets in the first step. Then a multi-layered structure is generated in the second step by bonding or welding laminates of different densities together [28]. Shimazaki et al. [29] investigated three-layer structures created by laminating ethylene-vinyl-acetate foam sheets to reduce the loads transmitted by shoe soles to the user during running and walking. By varying the concentration of the azodicarbonamide blowing agent (8, 12 and 16 phr), three different density layers (230, 170 and 110 kg/m^3) were foamed and laminated together and a 3-layer sandwich structure was produced with a total thickness of 15 mm. The shock absorption efficiency of the multilayer sandwich structures was evaluated by applying cyclic loads of 1000 N per second and placing pressure sensors in the top and bottom boundary layers. Their results showed that the use of functionally graded foams could advantageously modify the shock absorption of the system. In their case, samples with increasing density from top to bottom performed better, with the bottom layer taking the load first during running [29]. However, the deformation mechanisms in the foam layers were not investigated, so an accurate explanation of the results from a structural point of view is missing.

In summary, several modeling studies and experimental data have shown that density-graded polymeric foams can show enhanced energy absorption compared to single-density uniform structures. However, the reason for the positive effect of varying the density distribution is not fully understood, and the theories of previous research are not supported by experimental data. Furthermore, the typical testing methods of foams (compression test [30], drop weight impact test [31,32], Split Hopkinson Bar tests [33,34]) are not sufficient alone to give a detailed explanation of tendencies.

This study aims to investigate the impact loading of multi-layered functionally graded foam structures by developing a new measurement method based on the image processing of high-speed camera recordings. The high-speed (HS) camera is a commonly used tool for impact testing measurements to validate results and quantify maximum deformation [35]. For a similar research area, Hoohbor et al. [36] effectively used HS camera–based digital image correlation to analyze the stress wave propagation of high-velocity impacts from pressure Hopkinson bar tests with 3-layered rigid PU foams. They obtained the axial strains vs. time data to analyze the variation in the densification process of the structure as a function of the distance from the impact side. However, there is currently no measurement method available for the drop weight testing of polymeric foams that can monitor the deformed area's shape, size, and variation over time by treating the layers of different densities separately. While the current study focuses only on cross-linked polyethylene (XPE) foams used in the sports equipment industry, the method presented here can also be applied to

the design of foams for packaging and automotive industrial use.

2. Materials

We investigated discretely graded, three-layer, weakly cross-linked polyethylene foam structures. The foams had similar average densities but different densities in each layer. The cell-structural characteristics of the individual layers are summarized in Table 1. Cell density shows the number of the cells in a given volume. In general, the higher the cell density, the better the mechanical properties of the foam.

The foams were provided by Polifoam Ltd. (Budapest, Hungary). All structures were produced on a flat film production line with an azodicarbonamide foaming agent and a dicumyl peroxide cross-linking agent. The exact layer order of the functionally graded foam structures and their average densities are summarized in Table 2. The average densities were calculated from the specimens' mass and dimensions. In each case, the multilayer samples were welded together from three 10 mm thick layers by flame lamination. In the evaluation, all samples were compared to the uniform-density "50-50-50″ sample.

3. Experimental

3.1. Calculation of average density

The average densities of the structures were determined from the mass and dimensions of the specimens. The mass was measured with an Ohaus Explorer (Nänikon, Switzerland) balance (accuracy 0.0001 g), while the volume of the foam blocks was determined with a GOM ATOS Core 5 M (Gesellschaft für Optische Messtechnik GmbH, Germany) 3D optical measuring system.

3.2. Evaluation of shock absorption

3.2.1. Drop weight impact tests

The dynamic testing of the foams was carried out at four different impact energy levels with a Ceast 9350 impact tester using a 22 kN load cell. We varied impact energy by placing extra weights in the dropping frame. The exact measurement settings are summarized in Table 3.

The 100 × 100 × 30 mm size specimens were placed on a 40 mm thick steel plate, which functioned as rigid support during the impacts. When the cylindrical-shaped impactor was dropped down to the center of the foam, the force versus time data were recorded, from which the maximum reaction force, the maximum deformation, and the absorbed energy were calculated. Data was acquired with a Ceast DAS 64k High-Speed Data Acquisition Unit at 1 MHz.

3.2.2. Deformation analysis with a high-speed camera

A special arrangement was used to analyze the deformed area's shape, size, and variation over time. The structural deformation of the foam during impact testing was recorded with a Keyence VW-9000 high-speed camera. The schematics of the test setup are presented in Fig. 2.

We positioned the specimens with a dimension of 200 × 200 × 30 mm in such a way that only half of the impactor hits them, so that we can see the changes in the contours of the layers during deformation. The schematics shows only that part of the foam sample which is affected during the impact.

The measurement parameters were determined based on the results of preliminary tests, in which we varied the drop height and impactor mass until the deformation of the samples fell within the range of 80–100%. The finalized measurement settings were set to 400 mm drop height and 2.514 kg mass, which resulted in an impact energy of 9.86 J and impact velocity of 2.8 m/s. We investigated the deformation mechanism of the 3-layer foam structures with a new evaluation method based on the image analysis of the HS-camera recordings.

In this test, we prepared the samples in a special way, which made the segmentation of layers easier during image processing. The middle layer of the foams was masked with a tape, and an AESUB ASW102 white pigment spray was sprayed on the side of the foams. After the removal of the tape, a white-grey-white layer structure was formed (see Fig. 3).

Table 2
Layer order of the investigated foam structures.

Sample name	Nominal density of the top layer [kg/m^3]	Nominal density of the middle layer [kg/m^3]	Nominal density of the bottom layer [kg/m^3]	Average density [kg/m^3]
50-50-50	50	50	50	47.9 ± 0.5
30-50-70	30	50	70	48.7 ± 0.4
40-70-40	40	70	40	51.6 ± 0.7
70-30-70	70	30	70	54.4 ± 1.4
70-50-30	70	50	30	48.7 ± 0.4

Table 3
Test parameters of the impact tests.

Property	Value			
Impactor geometry	Cylinder			
Material of the impactor	Steel			
Impactor diameter	50 mm			
Drop height	400 mm			
Impact velocity	2.8 m/s			
Impactor mass	2.514 kg	3.514 kg	4.514 kg	5.514 kg
Impact energy	9.862 J	13.784 J	17.707 J	21.630 J

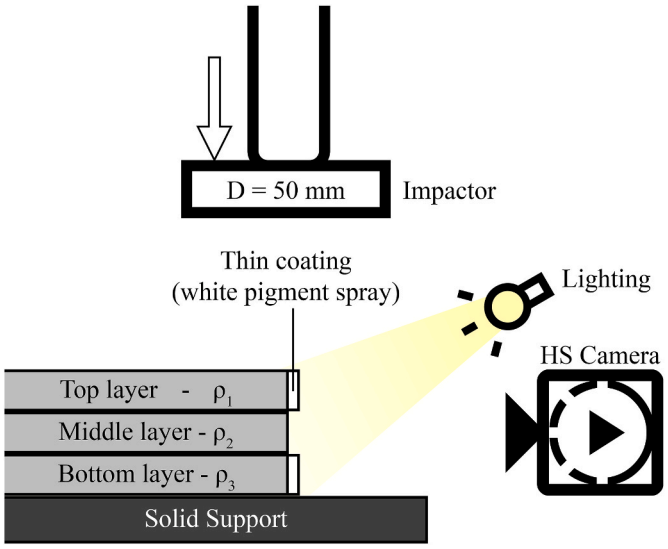

Fig. 2. Schematics of the test setup of impact testing with a high-speed camera (side view).

Table 1
Cell structural characteristics of the individual layers (based on our former study [13]).

Nominal density [kg/m^3]	30	40	50	70
Average cell size [μm]	622 ± 151	567 ± 163	500 ± 138	464 ± 108
Cell density [cells/cm^3]	2815	4194	4839	6947
Average cell wall thickness [μm]	6.7	8.7	9.1	12.3

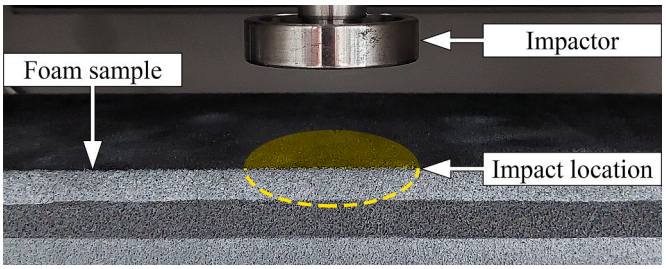

Fig. 3. Photo of the measurement layout with the white-grey-white layer structured sample (front view taken from the position of the high-speed camera).

We recorded the deformation with the high-speed camera during each impact at 2000 frames per second in 480 × 640 resolution, which means we took photos of the process every 0.5 ms. After recording, we extracted the process-related frames from the video files and investigated them. The steps of image processing can be seen in Fig. 4.

The first frame is when the impactor just touches the surface of the foam (where the Force–Deformation curves of the drop weight impact tests start). The last frame is when the penetration of the impactor is maximum (see Fig. 5/a). It is the same point where the Force–Deformation curve has a maximum.

The contour of the foam changes as a function of time during the impact and the deformation zone of the foam is not limited to the area under the dart. As a first step in defining the shape and the size of the deformed zone, we identified the pixels which belong to the foam. We

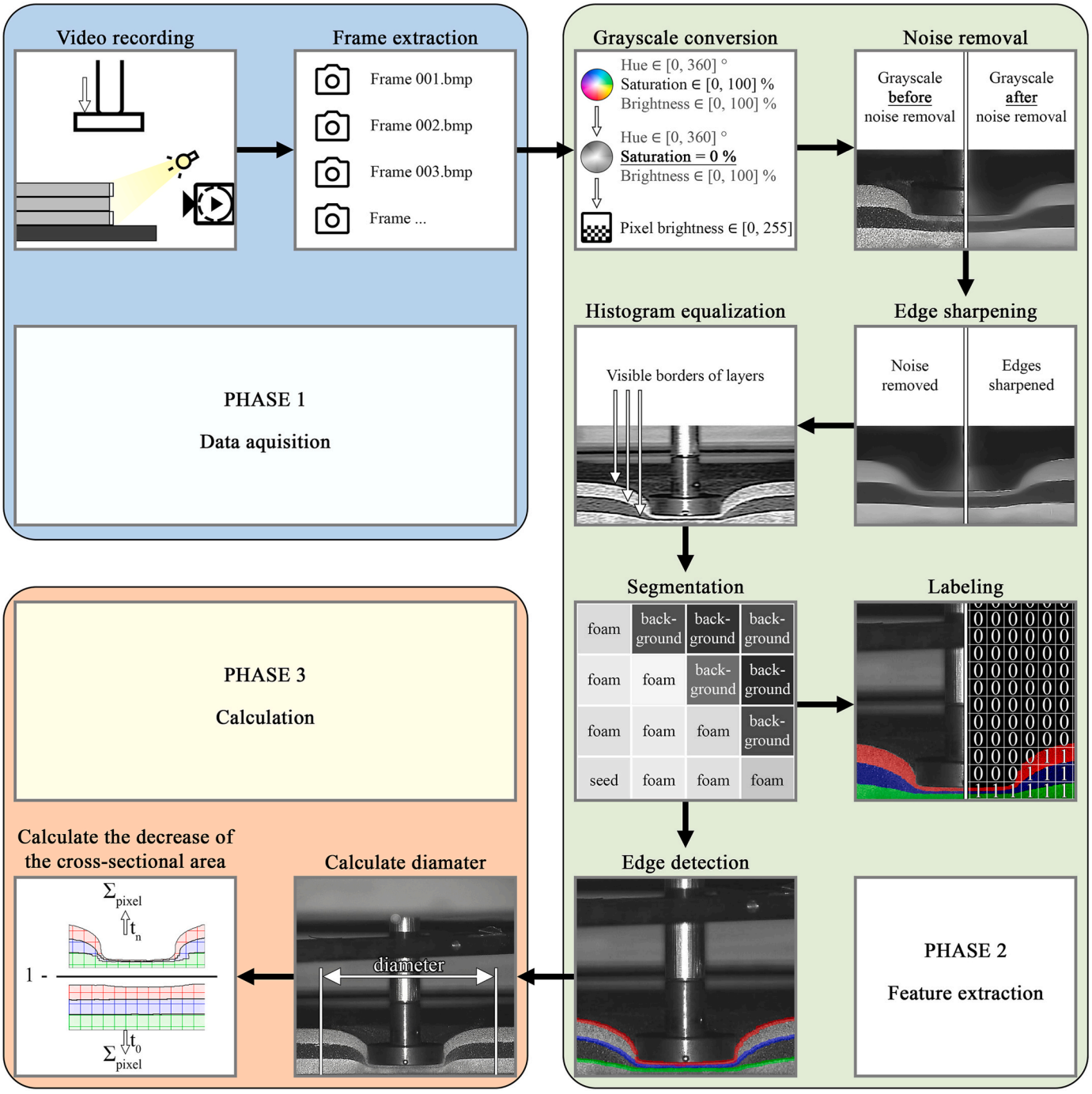

Fig. 4. Image processing flowchart.

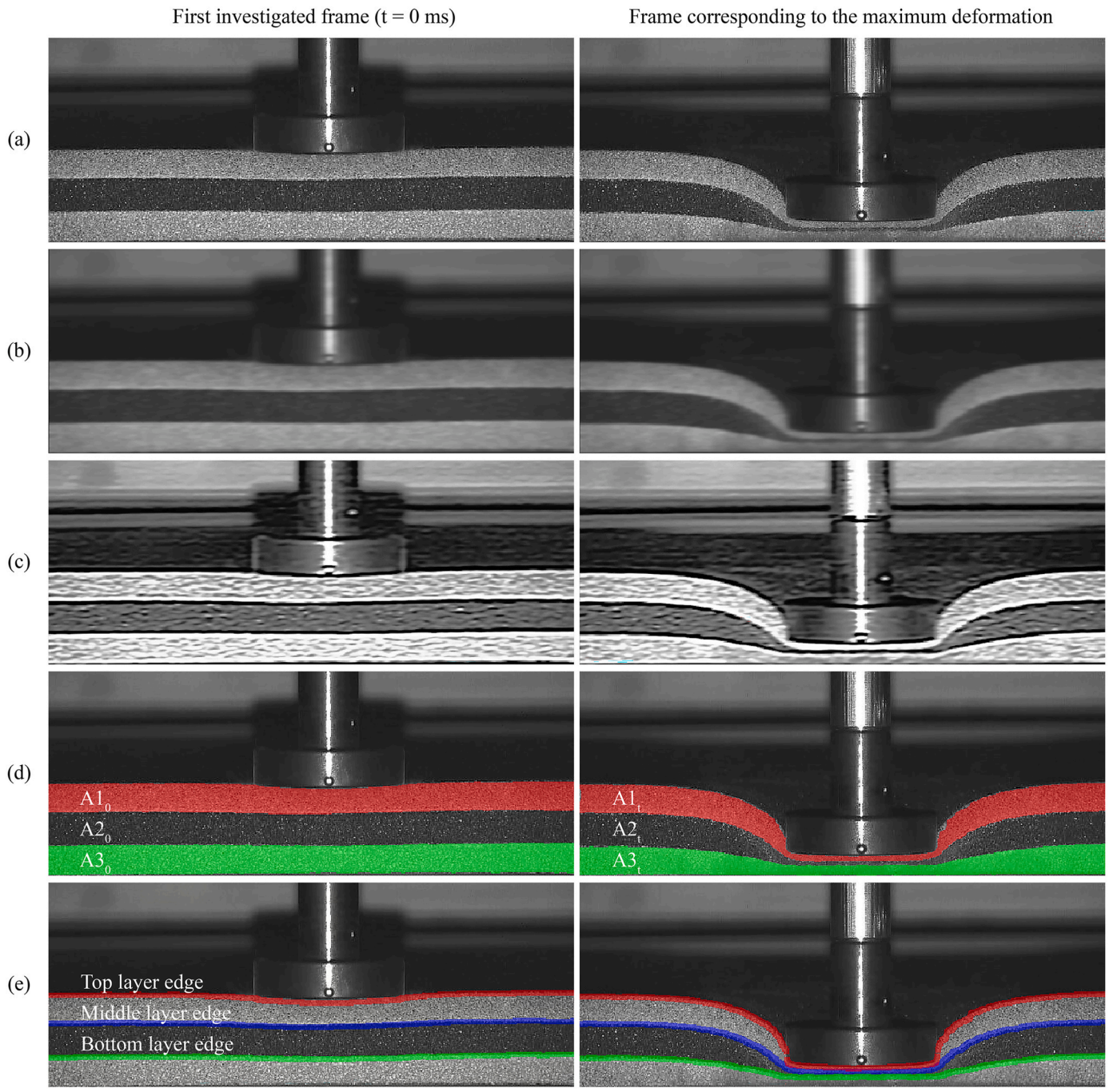

Fig. 5. Visualization of the image processing steps for the 70-50-30 sample: (a) original image, (b) noise removal, (c) edge sharpening and histogram equalization, (d) visualization of the label matrix, (e) labeling process of the edges.

used several image processing techniques to do that. We converted the extracted frames into grayscale images, where the color of the pixels is described as a number between 0 and 255, where the dark pixels have low intensity (Feature extraction step 1). The recorded video and the extracted frames were noisy, so the next step was noise removal. To remove noise, we used motion filters, which blur the original image (Fig. 5/b) The advantage of using the motion filters is that we can control the direction of blurring on the image so we can more or less preserve the contours of the layer edges.

The effect of noise removal also worsens the possibility of detecting the edges on the blurry images, which is why we used other filters on the frames to sharpen the edges and histogram equalization to increase contrast (Fig. 5/c).

It can be seen on the sharpened frames that the contours and the foam can be easily distinguished from the other part of the images. We used the so-called "Flood fill" segmentation to identify the pixels that belong to the foam. Flood fill segmentation requires a seed pixel, and it will investigate its neighborhood. Suppose the intensity of the neighboring pixel does not differ significantly from that of the seed pixel. In that case, it will be identified as foam, otherwise it will be background. The next step will investigate the neighbors connected to the pixels identified as foam and so on until all the pixels are examined. We used two seed points per layer on each side of the frame. The result of segmentation is a label matrix, whose size is the same as the frames and only contains zeros (not foam) and ones (foam). A separate label matrix belongs to each different foam layers. The visualization of the label

matrices can be seen in Fig. 5/d. The area of the layer cross-sections (A1, A2, A3) in pixels is the total number of pixels.

Based on the label matrices, we can extract the edges of the foam layers in every time step. We defined three important edges: top layer edge (top edge of the top layer), middle layer edge (top edge of the middle layer), and bottom layer edge (top edge of the bottom layer). The process visualization of the labeling of the edges can be seen in Fig. 5/e.

For example, the position of the top layer edge in the frame is the indices (vertical and horizontal position) of the first nonzero element in each column of the label matrix (Fig. 6). We defined the position of the edges every 0.5 ms for each layer. The changing of the top layer edge as a function of time can be seen in Fig. 7 in the case of the "70-50-30" foam.

To compare the different foam structures, we calculated two parameters that can describe deformation behavior. One of the parameters is the diameter of the deformed zone (Fig. 6) and the other is the decrease in the cross-sectional area of the foam layers. We calculated the diameter of the deformed zone from the vertical position of the edges. The vertical position $f(x,t)$ of the edges is a two-variable function whose value depends on the horizontal position and the time. For every time step, we calculated the difference ($d(x,t)$) between the actual vertical position and the starting position of the edges according to Equation (1).

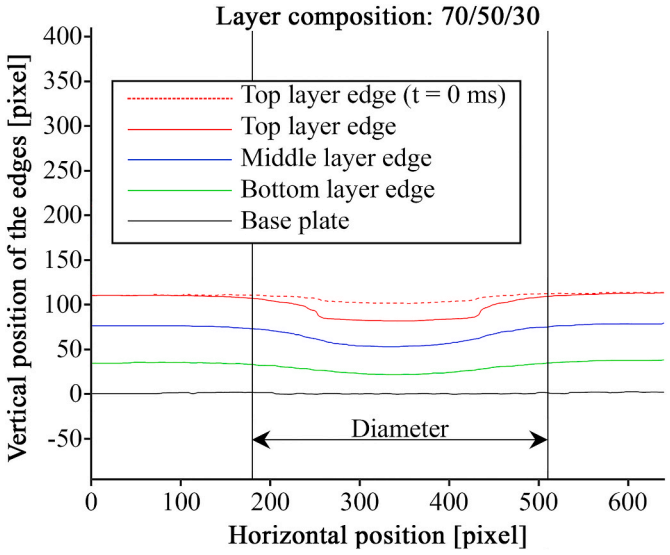

Fig. 6. The position of the edges at a given time.

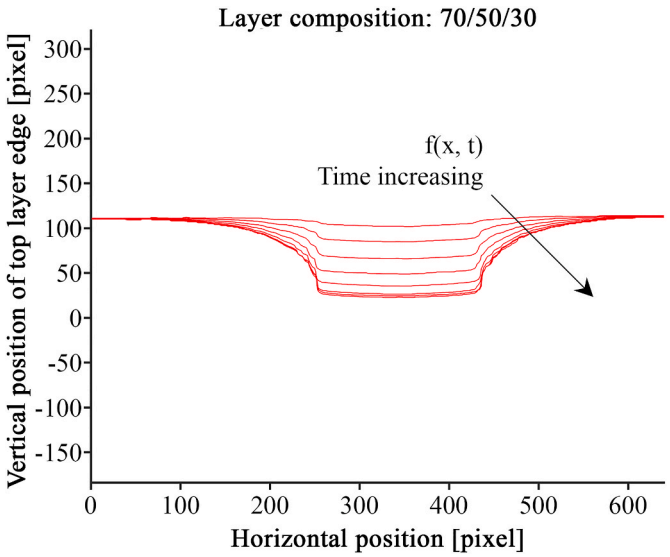

Fig. 7. The changing of the top layer edge as a function of time.

If the difference was bigger than 5 pixels, that part of the foam was deformed ($\varepsilon>5$). After we identified the deformed part of the edge, we extracted the horizontal position for the starting and the end point of the deformed part. The difference between these two is the diameter of the deformed part (Equation (2)). As we know the DPI of the frames, we were able to change the unit from pixels to mm. Each side of a pixel corresponded to a length of 0.2941 mm in our case. However, we must highlight that this ratio can vary significantly depending on the measurement setup, such as the distance between the camera and the object, and the resolution of the video recorder.

$$d(x,t) = f(x,0) - f(x,t) \tag{1}$$

$$D(t) = \max\,(x|d(x,t) > \varepsilon) - \min\,(x|d(x,t) > \varepsilon) \tag{2}$$

where $d(x,t)$ is the difference between the actual and starting vertical edge positions as a function of time, $f(x,0)$ is the vertical edge position at the first timestep and $f(x,t)$ is the actual vertical edge position as a function of time. $D(t)$ is the diameter of the deformed zone as a function of time and ε is a threshold limit, which we defined as 5 pixels.

The decrease in the cross-sectional area of the top layer at any time step can be calculated as the following (3):

$$\Delta A_t = \left(1 - \frac{A1_t}{A1_0}\right) * 100 \tag{3}$$

where ΔA_t [%] is the decrease in the cross-sectional area, $A1_0$ [mm^2] is the area of the cross-section of the top layer at the first time step, $A1_t$ [mm^2] is the cross-sectional area at a given time step. The calculation was the same for the middle and the bottom layers.

These two values can be used to compare the different foam structures and their deformation as a function of time.

4. Results and discussion

4.1. Drop weight impact tests

Fig. 8 shows the effect of increasing impact energy on the material response of the "50-50-50″ sample. All other samples had a similar trend of force-deformation curves.

In contrast to a typical quasi-static compression test where the whole specimen is compressed between two platens with a constant strain rate (see Fig. 1), we performed a dynamic test, in which the diameter of the impactor was only half of the specimen size. Therefore, the deformation of the foam in our case is heterogeneous. In addition, the foam's resistance is negligible compared to the magnitude of the load, so there is no significant initial elastic region. After an initial pre-loading stage, in the so-called plateau zone, the force does not remain constant and increases

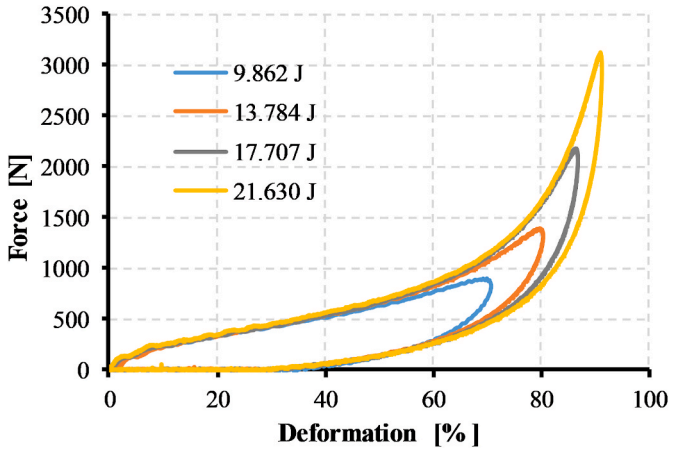

Fig. 8. Force–deformation curves of the "50-50-50″ sample for different impact energies.

linearly as the high strain rate contributes to the compression of the gas enclosed in the cells. Furthermore, the resistance to the impactor increases with the indentation depth due to the shear and compression deformation of the foam around the impactor head, which also increases the measured force. At larger strains, the nature of deformation changes, and the slope of the curve increases steadily. At this point, similar to the densification zone, the foam resists deformation significantly due to air compression and excessive compression of the cells [10,33].

For the smallest impact energy (9.862 J), the degree of deformation is optimal, as there is no final densification stage, and the nature of the deformation remains linear throughout the entire measurement. In this case, the samples stopped the downward movement of the dart before the foam structure became excessively compacted. However, as the impact mass—and hence the impact energy—increased, the last part of the curves (densification) became more significant. It is also visible that the increasing impact energy did not affect the slope of the curves at lower strains since the impact velocity was kept constant (constant drop height), and the impact energy was varied by modifying the weight of the impactor dropped onto the sample.

The results for absorbed energy (4), efficiency (5), maximum force, and maximum deformation derived from the curves are shown in Fig. 9.

$$E_{abs} = \int_0^{\varepsilon} F(\varepsilon)d\varepsilon \tag{4}$$

$$\eta = \frac{E_{abs}}{E_{imp}} \bullet 100 \tag{5}$$

where E_{abs} [J] is the absorbed energy, F [N] is the recorded force, ε [m] is the deformation, η [%] is the efficiency, while E_{imp} [J] is the impact energy.

Although the absorbed energy increased, the energy absorption efficiency (the ratio of absorbed energy to impact energy) decreased steadily as the drop weight was increased. The differently layered foam structures absorbed on average 79 ± 1% of the impact energy at the lowest impact energy level. With growing impact energy levels, this efficiency gradually decreased to 73 ± 1%, 70 ± 1%, and finally 67 ± 1%. This is due to the fact that the energy absorption efficiency of the foam decreases above a particular load since the rate of stress increase exceeds the rate of absorbed energy increase in the last part of the force–displacement curves [9].

Impact energy also significantly affected the maximum force generated during the impact. Regardless of the impact energy, the "70-50-30″ and "70-30-70″ layer orders showed the lowest maximum force. The "30-50-70″ specimen showed slightly higher maximum forces than the reference specimen ("50-50-50″), while the "40-70-40″ structure gave the worst results (highest force).

The maximum force results correlated well with the extent of mechanical damage in the samples as a result of impact. The samples that showed better shock absorption ("70-50-30" and "70-30-70") suffered negligible residual deformation. In contrast, in the case of the samples with high maximum force results, the foam suffered not only irreversible cellular, but external surface damages as well.

The maximum deformation of the tested samples also increased with increasing impact energy and appeared to approach a threshold limit. This is caused by more excessive cellular compaction due to higher impact energy. This assumes that at a given impact energy, the foam structures are already fully compressed, so further increasing the drop weight would not increase the maximum deformation but would cause an increase in the reaction force and produce more irreversible deformation in the cell structure.

Overall, the structures with a higher density foam layer at the side of the load showed the best shock absorption capacity, presumably due to the stiffer and more resistant top layer. The comparison of the force–deformation curves of the samples at the highest impact energy also supports this (see Fig. 10.).

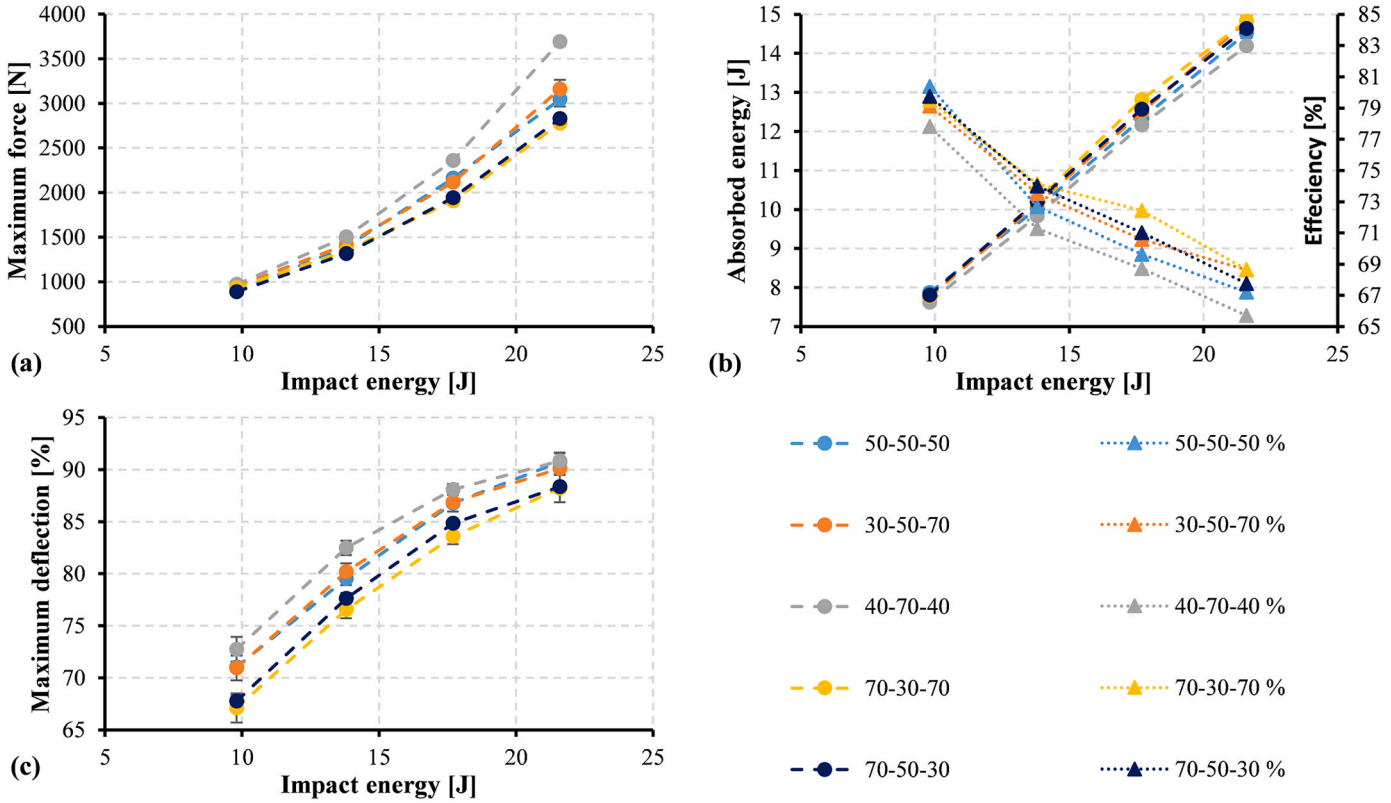

Fig. 9. Results of the impact tests for each sample: maximum force (a), absorbed energy (b) and maximum deformation (c).

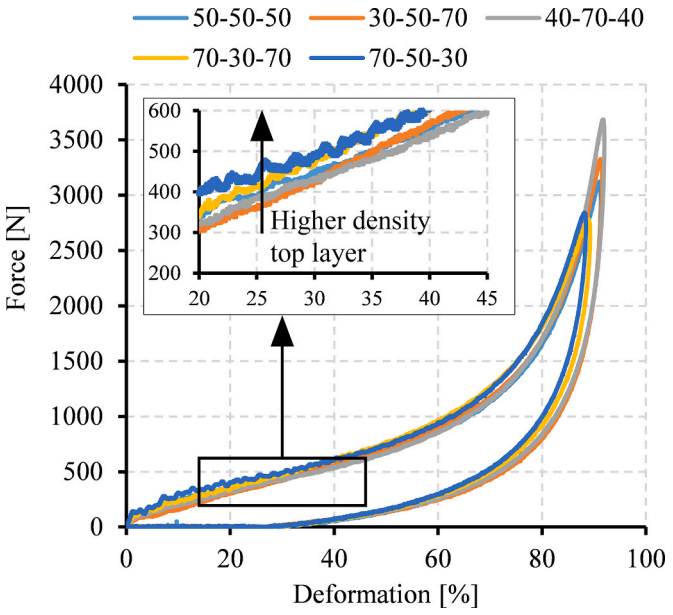

Fig. 10. Force–displacement curves of the samples at the impact energy of 21.630 J.

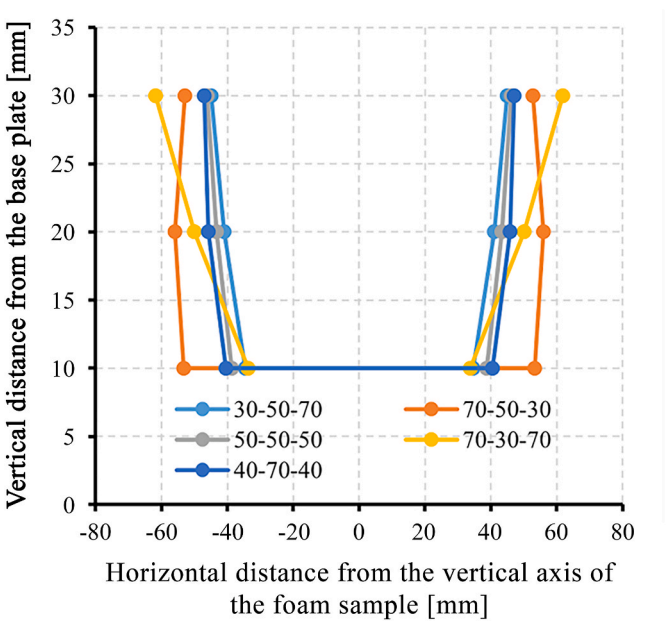

Fig. 11. Total area where cells undergo deformation.

It can be seen that the second phase of the curves of the "70-50-30″ and "70-30-70″ samples (70 kg/m^3 density top layer), which gave more favorable results, starts at a higher force due to the steeper initial pre-loading phase. Hence, they are able to absorb more energy before densification starts, which results in a smaller increase in the reaction force. For example, at 70% deformation, the "70-50-30″ sample absorbed 20 J of energy compared to 15 J absorbed by the "30-50-70″ sample. We assume that due to the higher stiffness of the 70 kg/m^3 top layer, the impact deformation mechanisms are less concentrated in the area just below the dart and the impact energy is distributed over a larger zone. However, the demonstration of this necessitated the taking of high-speed camera recordings and the development of a new evaluation method. Since the difference between the shock absorption capacity of the samples increased with increasing load, it can be concluded that the positive effect of the layer order modification appears mainly in the densification zone. For this reason, we set the measurement settings to achieve a high degree of deformation for each sample (above 80% strain) for high-speed camera recording.

4.2. *Investigating deformation with a high-speed camera*

By changing the variation of the layer order, the layers start to deform at different times and in a different order, which fundamentally affects the behavior of the foam. With image processing, we determined the outer points of the deforming zone for the top, middle and bottom edges. Plotting these points at the time of maximum deformation and connecting them gives a good approximation of the total volume involved in the deformation for the first two layers (see Fig. 11.). We assume that all cells in the area between the boundary lines are deformed, while no deformation has occurred outside the lines.

In addition, we determined the temporal variation of the decrease of the cross-sectional area and the diameter of the deforming zone, which properties have not been studied in the literature yet. In the following, the deformation mechanisms of each foam type will be discussed in detail.

4.2.1. *Homogeneous - density sample (50-50-50)*

For the homogeneous-density "50-50-50" sample (Fig. 12.), the progression of deformation is uniform, so the delay between the beginning of deformation in the top and middle and in the middle and

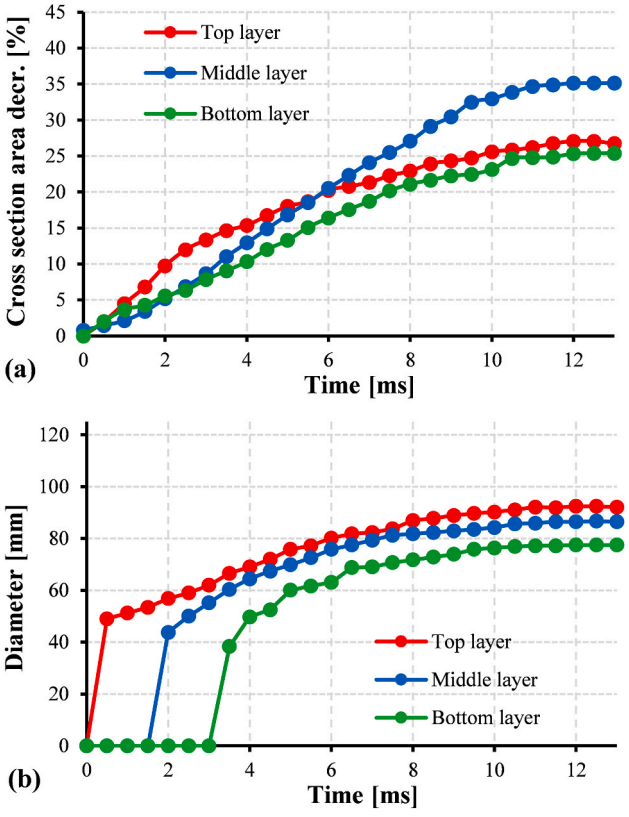

Fig. 12. Cross-sectional area decrease (a) and the diameter of the deforming zone (b) for the "50-50-50" structure.

bottom layers are identical. The magnitude of the cross-sectional area decrease differed noticeably among the top, bottom, and middle layers, although these differences were relatively small compared to the other samples with a non-uniform density distribution. Additionally, the shape of the curves was more similar in this sample. Their variation over time is initially linear, then the slope gradually decreases, due to the compaction of the cell structure, and it finally reaches a threshold. The saturation of the curves occurs simultaneously. The diameter of the deformation zone gradually decreases downwards from the top surface of the foam, with the number of cells involved in the deformation decreasing from layer to layer. Since the deformation zone is narrower in the bottom layer, the degree of compression in the cell structure is locally higher, which increases the reaction force recorded during drop weight testing.

4.2.2. 30-50-70 layered structure

The progression of deformation in the "30-50-70" layered system (Fig. 13.), which showed worse results in terms of shock absorption capacity, was different. In the first stage of the collision, the cross-sectional decrease is clearly the most significant in the top layer. Its variation over time was non-linear; the slope decreased steadily before reaching a threshold cross-sectional area reduction limit of around 27%. The underlying mechanism for this phenomenon is that the top layer's area under the impactor undergoes full compaction prior to significant deformation of the lower layers. This results in the load being initially concentrated on the top layer and then shifted to the middle layer once the top layer is fully compacted. Afterward, the cells in the middle layer also undergo full compaction, which leads to the load being concentrated on the densest bottom layer. Since the densification of the low-density top layer takes less time than the denser middle layer, the delay between the beginning of deformation in the top and middle layers is smaller than the delay between the middle and bottom layers. The diameter of the deformation zone also decreases from top to bottom, but the magnitude of this decrease is larger than in the uniform-density "50-50-50" sample.

4.2.3. 70-50-30 layered structure

The sample "70-50-30" (Fig. 14.), which has the highest density on the impact side and then decreasing density downwards, showed a deformation response opposite to the "30-50-70". The stiffer top layer immediately transfers the load to the underlying lower density middle layer, which is less resistant to mechanical loads, then this layer transmits it to the bottom least dense layer. Accordingly, all the layers start to be compressed at almost the same time without significant delay once the deformation process begins. For this reason, the degree of cross-sectional area reduction in the layers correlates with their density. The lowest-density bottom layer is compressed the most and the highest density top layer the least. A significant difference is that the diameter of the deformation zone is larger than in the "50-50-50" structure, and the width of the zone does not decrease from top to bottom. It results in far more cells being involved in energy absorption, so the degree of defor-

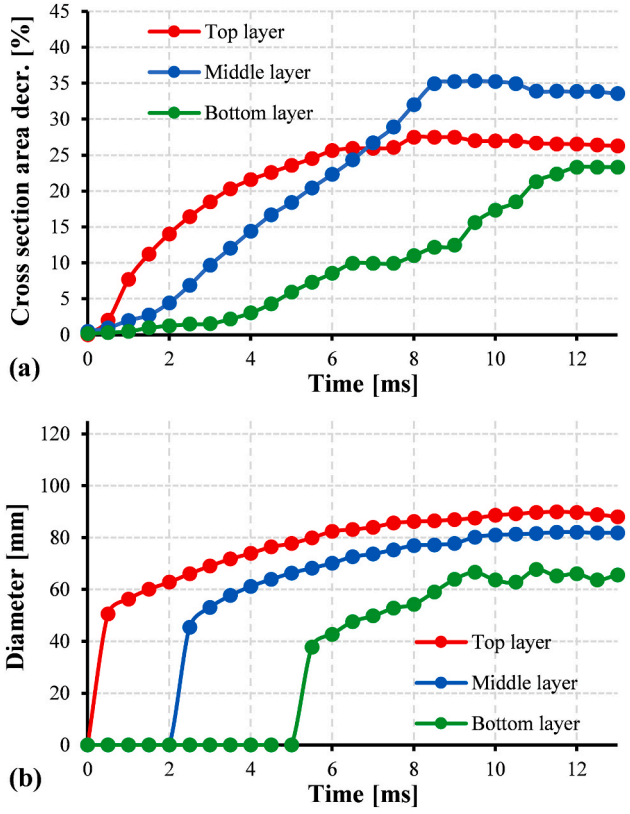

Fig. 13. Cross-sectional area decrease (a) and diameter of the deforming zone (b) for the "30-50-70" structure.

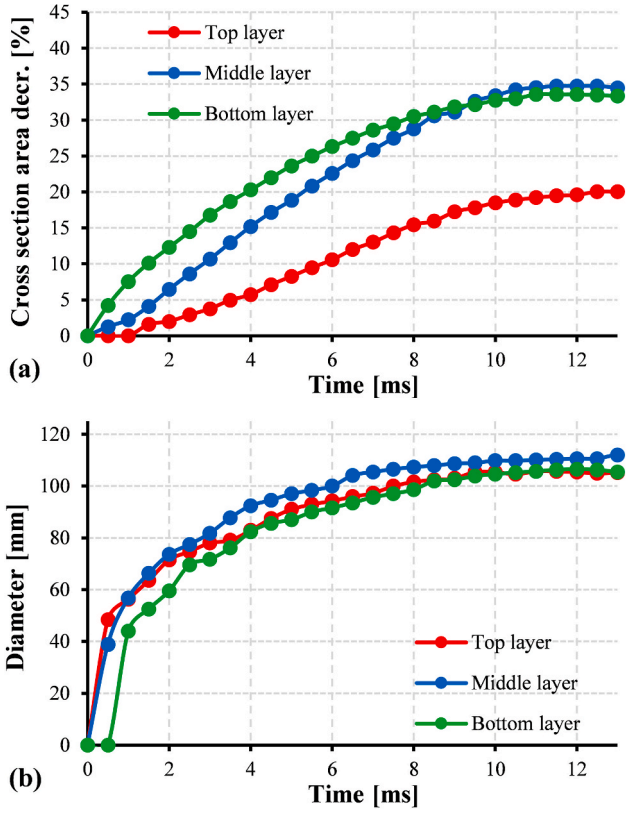

Fig. 14. Cross-sectional area decrease (a) and diameter of the deforming zone (b) for the "70-50-30" structure.

mation in each cell is smaller. Due to the typical nature of the compressive stress–strain curves of polymeric foams, this lower level of deformation results in a smaller maximum reaction force.

4.2.4. 70-30-70 layered structure

In the "70-30-70" sample (see Fig. 15.), the top high-density layer transmits the load to the less dense middle layer, causing both layers to undergo compression simultaneously. The deformation of the bottom, also dense layer, becomes more noticeable only after a relatively long time delay. Due to its lower density, the rate of the cross-sectional area decrease is clearly the greatest in the middle layer during the initial phase of the collision. Still, the upper layer also gradually loses its cross-sectional area. The variation in the cross-sectional area reduction over time in these layers is also similar to a saturation curve, with the low-density middle layer reaching a threshold value first (at about 8 ms), followed by the complete compaction of the top layer (at about 9 ms). The diameter of the deformation zone is the largest in the top layer, but the width of the zone decreases strongly from the top downwards. As the top and middle layers are deformed over a wide zone during the initial phase of the impact, this results in a higher stress plateau, similar to the "70-50-30" sample, which helps to absorb the impact energy at a relatively low maximum reaction force.

4.2.5. 40-70-40 layered structure

In the "40-70-40" sample (Fig. 16.), the striker impacted on a low-density layer with a denser layer located underneath. Thus, the top layer distributes most of the load to the middle layer only after the cell structure is compacted, with a time delay of about 1.5 ms. As the middle layer is compressed, it pushes down the bottom layer, resulting in simultaneous but varying rates of deformation in these two layers. Initially, the compression of the bottom layer is far more dominant, but once it reaches a threshold value, deformation progresses through the cellular compaction of the middle layer. The diameter of the deformation zone decreases from top to bottom at approximately the same rate as in the uniform-density "50-50-50" sample, which explains the similar magnitude of the maximum force results obtained in the regular drop weight tests.

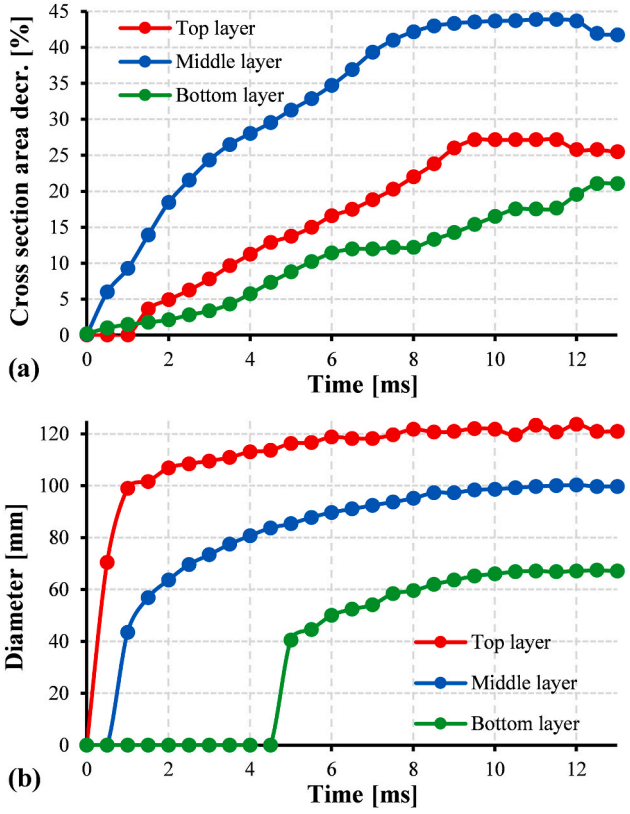

Fig. 15. Cross-sectional area decrease (a) and diameter of the deforming zone (b) for the "70-30-70" structure.

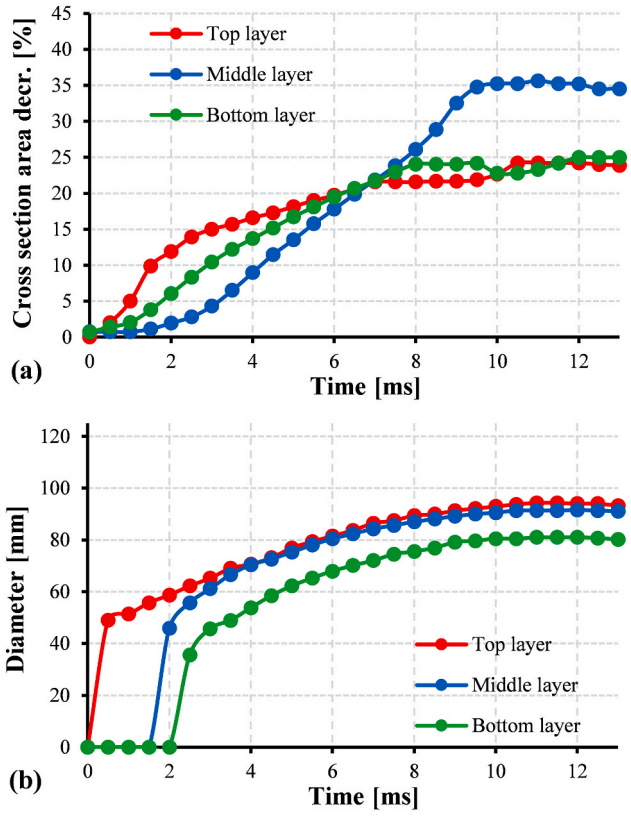

Fig. 16. Cross-sectional area decrease (a) and diameter of the deforming zone (b) for the "40-70-40" structure.

4.2.6. Summary of deformation characteristics

In summary, we can conclude that the variation of the layer order significantly affected the deformation response of the foam structures (see Table 4.). The use of layers with decreasing density from top to bottom contributes to the simultaneous deformation of the layers below each other. In contrast, if a low density layer is followed by a denser one, most of the deformation is concentrated in the top layer, and the deformation of the lower denser layers only becomes dominant after the densification of the top one. A high-density layer on the side receiving the impact also increases the diameter of the deformation zone. The time order of layer compaction depends mainly on foam density. As low-density layers have a less resistant structure (larger cells, thinner cell walls) to loads, full cellular compaction takes less time compared to higher density layers with smaller cells.

Table 4
Summary of the deformation characteristics of foam structures with different density variation.

Specimen type	Progression of deformation	Starting time of layer deformation[a] for top, middle, and bottom layers [ms]	Deforming zone diameter at the time of maximum deflection for top, middle and bottom layers [mm]	Time order of layer compaction
50–50–50	Stepwise (uniform time steps)	0	92.4	Simultaneous
		1.5	86.8	
		3.0	77.4	
70–50–30	All layers start to deform at the same time	0	105.7	1. Bottom
		0	112.0	2. Middle
		0.5	106.5	3. Top
30–50–70	Stepwise (increasing time steps)	0	89.9	1. Top
		2.0	82.1	2. Middle
		5.0	69.3	3. Bottom
70–30–70	Stepwise (increasing time steps)	0	123.6	1. Middle
		0.5	100.3	2. Top
		4.5	67.4	3. Bottom
40–70–40	Stepwise (decreasing time steps)	0	94.3	1. Top
		1.5	91.6	2. Bottom
		2.0	81.0	3. Middle

[a] (Starting time of layer deformation is calculated based on the temporal variation of the diameter of the deforming zone).

5. Conclusions

This study investigated functionally graded, three-layer, 30 mm thick weakly cross-linked polyethylene foam structures with the same average density (50 kg/m^3) but different densities in each layer. Based on the results of drop weight impact tests performed with a 50 mm diameter cylindrical impactor in the impact energy range of ~10–22 J, we showed that increasing the impact energy from 9.862 J to 21.630 J decreases the energy absorption efficiency of the foam structures from 79 ± 1% to 67 ± 1%. We also showed that the shock absorption of the foams could be improved by modifying the density distribution along the thickness. By applying a decreasing density variation from top to bottom, the maximum reaction force of the impact tests decreased by 7.09% compared to the foam structure with uniform density.

In order to analyze the deformation mechanism of each layer, we developed a new evaluation method based on an image processing algorithm, which can be used to quantify the size of the deformed area and its variation over time, and the number of cells involved in the deformation, by analyzing high-speed camera recordings in a MATLAB environment. Using the evaluation method, we demonstrated the positive effect of modifying the layer order on shock absorption capability. Decreasing density from top to bottom causes the top layer to transfer the load to the layer below, which transmits it to the bottom layer so that the cells in all three layers start to compress at the same time. In contrast, in the case of the uniform-density foam structure, there was a 1.5 ms time delay between the beginning of successive layer deformation. The high-density top layer is also more resistant to the impact and distributes the load over a 27.1% larger area, so cellular deformation takes place in a larger volume. The wider impact zone and the simultaneous deformation of the layers significantly increase the energy absorption capacity in the initial stage of deformation, as the ratio of volume fraction deforming under the densification strain is higher. As more cells absorb the load, the structure becomes more resistant, and the plateau of the force–deformation curve is shifted upwards by approximately 10%. This will increase the amount of energy absorbed by the end of the plateau zone, and the dart will have a lower velocity at the start of the densification zone. The downward movement of the dart stops sooner, thus reducing the degree of critical cell compaction, which would cause a significant increase in the reaction force.

As the test parameters in our study were limited to a narrow range of impact energies and the drop height was kept constant at 400 mm, further improvements may include extending the test parameters to higher impact energies and velocities where the whole cellular structure collapses irreversibly. The accuracy of the current measurement method can be further improved by using a higher-resolution high-speed camera. Additionally, the use of pressure measurement films positioned between the foam and support plate would allow us to also investigate the energy transferred to the plate. With the implementation of these improvements, further studies can contribute to a more comprehensive understanding of the deformation response of functionally graded foam structures.

CRediT author statement

Márton Tomin: Conceptualization, Methodology, Software, Formal analysis, Investigation, Validation, Writing - Original Draft, Supervision. Dániel Török: Methodology, Software, Formal analysis, Investigation, Data Curation, Writing - Review & Editing. Tamás Pászthy: Methodology, Software, Data Curation, Visualization, Writing - Review & Editing. Ákos Kmetty: Writing - Review & Editing, Supervision, Project administration, Funding acquisition.

Declaration of competing interest

The authors declare that they have no known competing financial interests or personal relationships that could have appeared to influence the work reported in this paper.

Data availability

The authors do not have permission to share data.

Acknowledgements

This research was supported by the Hungarian National Research, Development and Innovation Office (K 132462); and by United World Wrestling. The research reported in this paper is part of project no. BME-NVA-02, implemented with the support provided by the Ministry of Innovation and Technology of Hungary from the National Research, Development and Innovation Fund, financed under the TKP2021 funding scheme. Á. Kmetty is thankful for the support of János Bolyai Research Scholarship of the Hungarian Academy of Sciences. The authors are thankful for the foam samples to Polifoam Ltd. (Budapest, Hungary).

References

[1] N. Mills, Polymer Foams Handbook: Engineering and Biomechanics Applications and Design Guide, Elsevier Science, Oxford, 2007.

[2] C. Ge, Theory and practice of cushion curve: a supplementary discussion, Packag. Technol. Sci. 32 (2019) 185–197, https://doi.org/10.1002/pts.2427.

[3] S. Liu, J. Duvigneau, G.J. Vancso, Nanocellular polymer foams as promising high performance thermal insulation materials, Eur. Polym. J. 65 (2015) 33–45, https://doi.org/10.1016/j.eurpolymj.2015.01.039.

[4] S.A. Baghban, M. Khorasani, G.M.M. Sadeghi, Acoustic damping flexible polyurethane foams: effect of isocyanate index and water content on the soundproofing, J. Appl. Polym. Sci. 136 (2019), 47363, https://doi.org/10.1002/app.47363.

[5] J.C. Viana, Polymeric materials for impact and energy dissipation, Plast., Rubber Compos. 35 (2006) 260–267, https://doi.org/10.1179/174328906X146522.

[6] Y. Chen, R. Das, A review on manufacture of polymeric foam cores for sandwich structures of complex shape in automotive applications, J. Sandw. Struct. Mater. 24 (2022) 789–819, https://doi.org/10.1177/10996362211030564.

[7] Z.X. Zhang, Y.M. Wang, Y. Zhao, X. Zhang, A.D. Phule, A new TPE-based foam material from EPDM/PPB blends, as a potential buffer energy-absorbing material, Express Polym. Lett. 15 (2021) 89–103, https://doi.org/10.3144/expresspolymlett.2021.10.

[8] M. Tomin, Á. Kmetty, Polymer foams as advanced energy absorbing materials for sports applications—a review, J. Appl. Polym. Sci. 139 (2022), 51714, https://doi.org/10.1002/app.51714.

[9] M. Avalle, G. Belingardi, R. Montanini, Characterization of polymeric structural foams under compressive impact loading by means of energy-absorption diagram, Int. J. Impact Eng. 25 (2001) 455–472, https://doi.org/10.1016/S0734-743X(00)00060-9.

[10] L. Di Landro, G. Sala, D. Olivieri, Deformation mechanisms and energy absorption of polystyrene foams for protective helmets, Polym. Test. 21 (2002) 217–228, https://doi.org/10.1016/S0142-9418(01)00073-3.

[11] P.C.C. Pinto, V.R. da Silva, M.I. Yoshida, M.A.L. Oliveira, Synthesis of flexible polyurethane foams by the partial substitution of polyol by steatite, Polímeros 28 (2018) 323–331, https://doi.org/10.1590/0104-1428.10417.

[12] J.V. Mane, S. Chandra, S. Sharma, H. Ali, V.M. Chavan, B.S. Manjunath, R.J. Patel, Mechanical property evaluation of polyurethane foam under quasi-static and dynamic strain rates- an experimental study, Procedia Eng. 173 (2017) 726–731, https://doi.org/10.1016/j.proeng.2016.12.160.

[13] M. Tomin, Á. Kmetty, Evaluating the cell structure-impact damping relation of cross-linked polyethylene foams by falling weight impact tests, J. Appl. Polym. Sci. 138 (2021), 49999, https://doi.org/10.1002/app.49999.

[14] B. Koohbor, A. Kidane, Design optimization of continuously and discretely graded foam materials for efficient energy absorption, Mater. Des. 102 (2016) 151–161, https://doi.org/10.1016/j.matdes.2016.04.031.

[15] N. Gupta, E. Woldesenbet, Microballoon wall thickness effects on properties of syntactic foams, J. Cell. Plast. 40 (2004) 461–480, https://doi.org/10.1177/0021955x04048421.

[16] N. Gupta, A functionally graded syntactic foam material for high energy absorption under compression, Mater. Lett. 61 (2007) 979–982, https://doi.org/10.1016/j.matlet.2006.06.033.

[17] M. Higuchi, T. Adachi, Y. Yokochi, K. Fujimoto, Controlling of distribution of mechanical properties in functionally-graded syntactic foams for impact energy absorption, Mater. Sci. Forum 706–709 (2012) 729–734. https://doi.org/10.4028/www.scientific.net/MSF.706-709.729.

[18] A. Mohyeddin, A. Fereidoon, A semi-empirical model for density gradient in microcellular thermoplastic foams, J. Cell. Plast. 47 (2011) 413–428, https://doi.org/10.1177/0021955X11406003.

[19] J. Yu, L. Song, F. Chen, P. Fan, L. Sun, M. Zhong, J. Yang, Preparation of polymer foams with a gradient of cell size: further exploring the nucleation effect of porous inorganic materials in polymer foaming, Mater. Today Commun. 9 (2016) 1–6, https://doi.org/10.1016/j.mtcomm.2016.08.006.

[20] E. Cusson, A. Akbarzadeh, D. Therriault, D. Rodrigue, Density graded polyethylene foams: effect of processing conditions on mechanical properties, Cell, Polym 38 (2019) 3–14, https://doi.org/10.1177/0262489319839632.

[21] C. Tovar-Cisneros, R. González-Núñez, D. Rodrigue, Effect of mold temperature on morphology and mechanical properties of injection molded HDPE structural foams, J. Cell. Plast. 44 (2008) 223–237, https://doi.org/10.1177/0021955x07088044.

[22] A.N.J. Spörrer, V. Altstädt, Controlling morphology of injection molded structural foams by mold design and processing parameters, J. Cell. Plast. 43 (2007) 313–330, https://doi.org/10.1177/0021955x07079043.

[23] J. Gómez-Monterde, M. Schulte, S. Ilijevic, J. Hain, D. Arencón, M. Sánchez-Soto, M.L. Maspoch, Morphology and mechanical characterization of ABS foamed by microcellular injection molding, Procedia Eng. 132 (2015) 15–22, https://doi.org/10.1016/j.proeng.2015.12.462.

[24] K.Z. Uddin, G. Youssef, M. Trkov, H. Seyyedhosseinzadeh, B. Koohbor, Gradient optimization of multi-layered density-graded foam laminates for footwear material design, J. Biomech. 109 (2020), 109950, https://doi.org/10.1016/j.jbiomech.2020.109950.

[25] M. Tomin, A. Kossa, S. Berezvai, Á. Kmetty, Investigating the impact behavior of wrestling mats via finite element simulation and falling weight impact tests, Polym. Test. 108 (2022), 107521, https://doi.org/10.1016/j.polymertesting.2022.107521.

[26] L. Cui, S. Kiernan, M.D. Gilchrist, Designing the energy absorption capacity of functionally graded foam materials, Mater. Sci. Eng., A 507 (2009) 215–225, https://doi.org/10.1016/j.msea.2008.12.011.

[27] S.T. Lee, Foam Extrusion: Principles and Practice, CRC Press, London, 2000.

[28] E. Shim, Bonding requirements in coating and laminating of textiles, in: I. Jones, G. K. Stylios (Eds.), Joining Textiles, Woodhead Publishing, Cambridge, 2013, pp. 309–351.

[29] Y. Shimazaki, S. Nozu, T. Inoue, Shock-absorption properties of functionally graded EVA laminates for footwear design, Polym. Test. 54 (2016) 98–103, https://doi.org/10.1016/j.polymertesting.2016.04.024.

[30] M.C. Saha, H. Mahfuz, U.K. Chakravarty, M. Uddin, M.E. Kabir, S. Jeelani, Effect of density, microstructure, and strain rate on compression behavior of polymeric foams, Mater. Sci. Eng., A 406 (2005) 328–336, https://doi.org/10.1016/j.msea.2005.07.006.

[31] G. Lyn, N.J. Mills, Design of foam crash mats for head impact protection, Sports Eng. 4 (2001) 153–163, https://doi.org/10.1046/j.1460-2687.2001.00081.x.

[32] A. Kmetty, M. Tomin, T. Barany, T. Czigany, Static and dynamic mechanical characterization of cross-linked polyethylene foams: the effect of density, Express Polym. Lett. 14 (2020) 503–509, https://doi.org/10.3144/expresspolymlett.2020.40.

[33] S. Ouellet, D. Cronin, M. Worswick, Compressive response of polymeric foams under quasi-static, medium and high strain rate conditions, Polym. Test. 25 (2006) 731–743, https://doi.org/10.1016/j.polymertesting.2006.05.005.

[34] B. Song, W. Chen, X. Jiang, Split Hopkinson pressure bar experiments on polymeric foams, Int. J. Veh. Des. 37 (2005) 185–198, https://doi.org/10.1504/ijvd.2005.006656.

[35] B.F. Berencsi, A. Kossa, Analyzing the effect of temperature on squash ball impacts using high-speed camera recordings, Period. Polytech. - Mech. Eng. 65 (2021) 354–362, https://doi.org/10.3311/PPme.18381.

[36] B. Koohbor, S. Ravindran, A. Kidane, In situ deformation characterization of density-graded foams in quasi-static and impact loading conditions, Int. J. Impact Eng. 150 (2021), 103820, https://doi.org/10.1016/j.ijimpeng.2021.103820.